Mid-Century Changes in the Mean and Extreme Climate in the Kingdom of Saudi Arabia and Implications for Water Harvesting and Climate Adaptation

atmosphere

MDPI

Article

Mid-Century Changes in the Mean and Extreme Climate in the Kingdom of Saudi Arabia and Implications for Water Harvesting and Climate Adaptation

Muge Komurcu [1,*], C. Adam Schlosser [1], Ibtihal Alshehri [2], Tariq Alshahrani [2], Waleed Alhayaza [2], Adnan AlSaati [2] and Kenneth Strzepek [1]

[1] Massachusetts Institute of Technology, Joint Program on the Science and Policy of Global Change, Center for Global Change Science, Cambridge, MA 02139, USA; casch@mit.edu (C.A.S.); strzepek@mit.edu (K.S.)

[2] Center for Complex Engineering Systems, King Abdulaziz City for Science and Technology, Riyadh 11442, Saudi Arabia; ibtihal@mit.edu (I.A.); t.alshahrani@cces-kacst-mit.org (T.A.); alhayaza@mit.edu (W.A.); adnana@mit.edu (A.A.)

* Correspondence: muge@mit.edu

Received: 22 July 2020; Accepted: 3 October 2020; Published: 8 October 2020

Abstract: The Kingdom of Saudi Arabia (KSA) is a water-scarce region with a dry, desert climate, yet flood-producing precipitation events and heat extremes lead to loss of life and damages to local infrastructure, property and economy. Due to its distinctive natural and man-made spatial features (e.g., coastal features, wadis, agricultural areas) studying changes in the mean climate and extreme events requires higher-resolution climate projections than those available from the current generation of Earth System Models. Here, a high-resolution convection-permitting regional climate model is used to downscale the middle of the 21st century (2041–2050) climate projections of the Community Earth System Model (CESM) under representative concentration pathway (RCP) 8.5 and for a historical time period (2008–2017) focusing on two months (August and November) within KSA's dry-hot and wet seasons, where extreme events have historically been observed more frequently. Downscaling of climate reanalysis is also performed for the historical time period (2008–2017) to evaluate the downscaling methodology. An increase in the intensity and frequency of precipitation events is found in August by mid-century, particularly along the mountainous western coast of KSA, suggesting potential for water harvesting. Conversely, the northern flank of the Empty Quarter experiences a noticeable reduction in mean and extreme precipitation rates during the wet season. Increasing August heat index is found to particularly make regional habitability difficult in Jeddah by mid-century.

Keywords: convection-permitting regional climate modeling; climate projections; Arabian Peninsula; climate extremes; water harvesting

1. Introduction

The Kingdom of Saudi Arabia (KSA) has a dry, hot climate with infrequent rainfall (e.g., [1]). Several studies show increasing trends in temperatures in station observations across KSA (e.g., [2–5]) as well as in gridded observational products (e.g., [6]). For example, Almazroui et al. (2014) investigated the trends of extreme temperatures in Saudi Arabia using observations from 27 ground-based stations for 30 years (1981–2010) and found that temperature extremes were higher in magnitude and more frequent for both cold and warm extremes during the most recent decade (1996–2010) of their analysis [4]. They also reported a greater than 90% increase in the annual number of warm days and

nights, along with similar reductions in cool days/nights between the two time periods (1996–2010 and 1981–1995). Furthermore, the region's already hot climate is projected to get warmer under climate change (e.g., [7–9]). Increasing temperatures and evapotranspiration rates are expected to have significant effects on the Kingdom's already scarce water resources and make it difficult to source agricultural, industrial and domestic water demands [1]. Combined effects of increasing temperatures and humidity also pose threats to the continuation of life and daily activities of humans (e.g., [10]). Using regional climate modeling at coarse, 25 km horizontal resolution, Pal and Eltahir (2016) found that the majority of the Arabian Peninsula (AP) is likely to become uninhabitable by the end of the 21st century under a high-impact emissions scenario (Representative Concentration Pathway (RCP) 8.5) due to a combination of increasing temperatures and humidity [11].

Precipitation is scarce in the AP. Based on an analysis of 28 ground-based meteorological stations in KSA for a ~30-year time period (~1970s to 2003), Mashat and Bassett (2011) found that the highest annual rainfall amounts are observed in the boreal spring in the southwest, west and east of the Kingdom, while the second-highest rainfall amounts occur over the boreal winter in the east and northeast [12]. Using station observations and gridded observational datasets, Almazroui et al. (2012) showed decreasing rainfall trends in KSA and most of the AP over the historical time period between 1978 and 2009, while southern part of the peninsula along the coast of Red Sea showed an increase [3]. Despite its desert climate, short-duration (3–5 h) intense bursts are known to comprise much of the total annual rainfall of a subregion (e.g., [3]), and several major cities in KSA experience extreme precipitation events that lead to flooding [1,13,14]. Recent frequent extreme precipitation events in Riyadh, the capital city, and Jeddah claimed several hundred lives, hundreds of residents went missing and these events led to significant damage to infrastructure and regional economy (e.g., USD 1 billion in monetary losses and USD 1.5 billion in damages and compensation for Jeddah floods in 2009) [15,16]. In Jeddah, the highest number of these extreme precipitation events occurred in November over the 1978–2012 time period [1]. Between 1970 and 2014, the largest amount of average monthly rainfall per year was experienced in November [16].

In addition to building resilience to future flooding events, studying potential future changes in precipitation rates is also important for the replenishment of water resources such as groundwater aquifers, which are the main source of water in KSA [1]. Previous studies suggested rainwater and runoff harvesting as a means to increase sources of water supplies in arid regions under climate change (e.g., [17]). To explore the feasibility of such adaptation techniques, it is essential to study the sub-regional, local and seasonal changes in precipitation rates with climate change. Furthermore, incidences of infectious diseases such as malaria are known to increase in the region after heavy rainfall and flooding events [1,18]. Studies of future changes in mean and extreme precipitation rates in the region, however, reveal differences across subregions with increasing model resolution and conclude that high-resolution simulations are needed for better representation of extreme precipitation events (e.g., [8]).

Several studies were performed to assess future climate change in the region using Earth System Model (ESM) projections as well as dynamical downscaling of ESMs using regional climate models (e.g., [6,8,9,11,19]). While these studies were useful to understand and reveal potential changes in climate and the complexities associated with representing the unique spatial features of KSA, the horizontal resolutions of these studies were too coarse to study changes in climate in local scales and to be used in local-scale adaptation studies. Furthermore, none used convection-permitting regional climate modeling (≤4 km horizontal resolution). High-resolution, convection-permitting simulations of synoptic events in the region were, on the other hand, shown to add value in simulating extreme rainfall and the convective features of flash-flood-producing storm events in Jeddah [20]. Climate change information at high spatial resolution can provide valuable insights towards the assessment of potential risks due to climate change and changing extremes and further inform actions that support increased local resiliency. Studying the range of potential changes in the mean and extreme temperatures and precipitation rates at local, city scales are, therefore, of significant importance for

the sustainability of regional communities and economies as well as regional habitability in KSA. In this study, we aim to (1) study regional and local changes in the climate of KSA by the middle of the 21st century under a high-impact emission scenario and (2) provide insights to regional scientists, engineers, decision-makers and stakeholders with high-resolution climate change information that can inform local and regional adaptation and resilience studies. To assess changes in regional and local climate in KSA, we use a very-high-resolution (4 km horizontal resolution), convection-permitting climate modeling approach for dynamical downscaling of ESM projections. In a study similar to ours, using 4 km horizontal resolution simulations, Alsarraf and Brooke (2015) investigated mid-century changes in summertime wind speeds [21]. Their simulations, however, cover only a portion of the AP at 4 km resolution, are of short (5-year) duration, focus on future changes in winds only (not temperatures or precipitation rates) and are not convection-permitting [21]. Removing convection parameterization is a distinctive feature of our simulations that, to our knowledge, none of the regional climate modeling studies focusing on climate change in KSA and the AP have previously taken advantage of. A discussion of advantages of removing convection parameterization in regional climate models is provided in [22]. Due to the substantial computational resources required to perform regional climate simulations at convection-permitting scales (e.g., [22]), we are only able to downscale a single ESM under a high-impact emission scenario and simulate two months that fall within the dry-hot and wet seasons across KSA [23]: August and November, respectively. These months have also historically been shown to contain the most frequent and intense heat and precipitation events in the region, respectively (e.g., [1]). While 10 years is too short to make climatologically robust statements, and downscaling of more ESMs under different scenarios is needed to provide a comprehensive picture of changes in climate, our aim with this study is to highlight the potential usage of this computationally expensive modeling to not only produce high-resolution projections that are able to capture the effects of unique local spatial features but also the use of such projections in creating local solutions for climate adaptation in the region.

In Section 2, we describe our modeling methodology and briefly describe the datasets used in our study. We evaluate our methodology and present the projected changes in the climate of KSA by mid-century using our high-resolution modeling in Section 3. We discuss our results in Section 4.

2. Methodology and Experiments

2.1. Regional Climate Model Configuration

The dynamical downscaling is based on the methodology used in Komurcu et al. (2018) [22]: We use bias-corrected Community Earth System Model (CESM) v1.0 projections under RCP 8.5 [24,25] as initial and boundary conditions in the Weather Research and Forecasting Model (WRF) v3.6.1 [26] with three nested domains of 36, 12 and 4 km horizontal resolution (Figure 1) with 40 vertical atmospheric levels. WRF has been extensively used for weather forecasting and atmospheric research as well as for dynamical downscaling of climate reanalyses and climate projections to study historical climate and future climate change (e.g., [22,27–29]). Similar to Komurcu et al. (2018) [22], we perform convection-permitting simulations, meaning that we use convection parameterization (Kain–Fritsch (K–F) [30]) only in domains 1 and 2 and no convection parametrization is used in domain 3. Use of K–F in WRF has been evaluated and shown to yield reasonable spatial distributions as well as temperature and precipitation patterns similar to observed climatology in the AP [29]. While our highest resolution domain (see Figure 1) includes parts of several countries in the AP, our simulations and analysis are focused on the Kingdom of Saudi Arabia. The parameterization setup of our simulations is the same as that of Komurcu et al. (2018) [22], with one exception. For the microphysics parameterization, we enable a single moment parametrization, the WRF Single Moment 6-Class Microphysics Scheme (WSM6) [31], after benchmarking tests indicated a considerable improvement in computational efficiency with no loss to model performance when simulating observed precipitation for this region. We use Community Land Surface Model (CLM) v4 [32] for the land surface scheme, Yonsei University scheme [33] for the

planetary boundary layer scheme and Rapid Radiative Transfer Model (RRTMG) [34] for short- and longwave radiation parameterizations. Similar to Komurcu et al. (2018) [22], in our simulations, we use two-way feedback between the nested domains, and, consistent with the driving ESM, greenhouse gas concentrations increase with time following RCP 8.5 emissions. Similar to Komurcu et al. (2018) [22], we perform monthly simulations with a 15-day re-initialization time period, which we discard, and we generate hourly output.

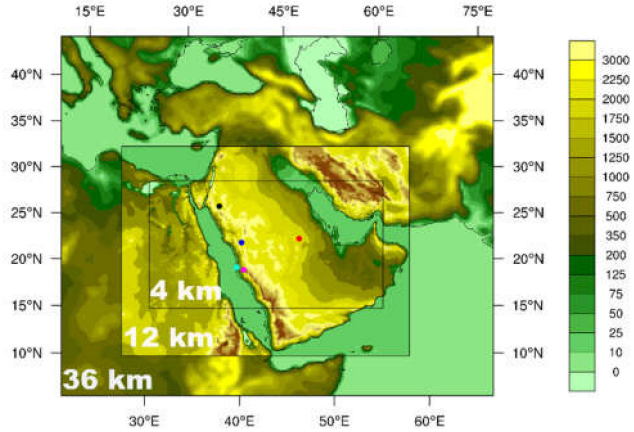

Figure 1. Three nested domains of 36, 12 and 4 km horizontal resolution and topography [m] used in our Weather Research and Forecasting Model (WRF) simulations. Markers represent locations of five local sites used in the analysis. Red: Riyadh, Black: Tabuk, Navy: Madinah, Cyan: Jeddah, Magenta: Makkah.

During our analysis, we performed local assessments of climate change at five strategic locations in the region; these locations are marked on Figure 1. The locations are selected based on discussions with our local co-authors and comprise populated, economically important sites as well as future touristic and historically significant destinations, all of which have been and are expected to be susceptible to effects of climate change and changing extreme climate events. The five local sites are Riyadh, the capital city (where intense heat waves and floods have been observed); Makkah and Madinah, destinations of religious tourism (i.e., Hajj, Umrah and Ziyarah); Jeddah, a historically preserved, populous coastal city (where frequent and deadly floods have occurred); and Tabuk, a designated future touristic site with relaxed laws to attract global tourism, which is part of a push by the leadership to reduce the Kingdom's economic dependency on oil.

2.2. Numerical Experiments and Supporting Data

Downscaling of CESM output using WRF has been performed for both middle of the 21st century climate under RCP 8.5 (2041 to 2050) (WRF-MC) and a historical time period (2008 to 2017) representative of present-day (PD) climate (WRF-PD). These two simulation sets are used to assess the potential changes in mean climate and extreme events by mid-century. We use six-hourly bias-corrected [24,25] CESM fields at a ~1° horizontal resolution. The input CESM data are available at NCAR's Computational Information Systems Laboratory (CISL) Research Data Archive (RDA) [35].

We also performed downscaling of the European Centre for Medium Range Weather Forecasting (ECMWF) Interim (ERA-Interim) Reanalysis using the same model setup for the historical time period (2008–2017) (WRF-ERA) to evaluate the ability of the model setup to replicate observed historical climate. We use six-hourly ERA-Interim data [36] not only to drive our historical WRF simulations, but also to assess the impact of the downscaling and the enhanced resolution of the WRF sub-domains. The ERA-Interim dataset is available at NCAR CISL's RDA [37]. We choose ERA-Interim as our driver field because ERA-Interim was, at the time of simulations, one of the best available reanalysis products (e.g., [22,38]). Furthermore, both ERA-Interim and its predecessor ERA-40 have been extensively used

in similar downscaling studies focusing on analysis of regional climate change across different regions around the world and as proxy for observations (e.g., [20,26,37–40]); most importantly, they have been used in this context over the AP (e.g., [6,11,41]).

The names and descriptions of the numerical experiments performed in this study are listed in Table 1.

Table 1. Numerical experiments undertaken in this study.

Experiment	Experiment Description	Experiment Duration
WRF-ERA	ERA-Interim driven WRF simulations	2008–2017
WRF-PD	CESM RCP8.5 driven WRF Historical simulations	2008–2017
WRF-MC	CESM RCP8.5 driven Mid-Century simulations	2041–2050

High-resolution climate products, particularly precipitation fields, are difficult to evaluate due to a lack of comparable-resolution observational and reanalysis products and also due to observational uncertainties (e.g., [22,42–44]). Hence, quantitative differences in precipitation rates between our high-resolution WRF simulations (at 4 km) and observed/retrieved/reanalyzed products are expected due to distinct features of the latter products—such as smoothing of precipitation rates due to coarser resolution, spatially non-homogeneous measurements, uncertainties in retrieval algorithms and interpolation methods, which are explained in depth in previous literature (e.g., [22,42–44]). To address this issue, we use a variety of observations-based/retrieved/reanalyzed gridded products with different horizontal resolution to evaluate our WRF downscaled fields: precipitation rates from the Global Precipitation Measurement (GPM) [45] and Climate Research Unit (CRU) [46] and temperatures from ERA5 [47]. Precipitation rates from GPM have 0.1° horizontal resolution and provide precipitation retrievals based on a constellation of satellites [31]. We use the daily Integrated Multi-Satellite Retrievals for GPM (IMERG) final precipitation L3 product (3B-DAY.MS.MRG.3IMERG v06) [48] which is available online from NASA at https://giovanni.gsfc.nasa.gov/giovanni/. We also use precipitation rates from the Climatic Research Unit gridded time series (CRU TS) version 4 [46], which includes interpolation of monthly climate variables from global station observations. CRU version 4 has 0.5° spatial resolution and is available for download at https://crudata.uea.ac.uk/cru/data/hrg/. ERA5 [47] is the latest version of climate reanalysis product replacing ERA-Interim and has a horizontal resolution of 31 km, which is a significant improvement over the 80 km resolution of its predecessor. Due to its higher resolution and its advancement over ERA-Interim, we use daily temperatures from ERA5 to assess the biases in our downscaled fields. The ERA5 dataset is also available at NCAR CISL's RDA [49].

Due to the heavy computational cost associated with our convection-permitting regional climate modeling, we perform simulations for two months (November and August) representative of wet (November–April) and dry-hot (May–October) seasons, respectively (e.g., [23]). We pick these two months based on the results of previous published work on historical climate analysis of KSA (e.g., [1,16]) (particularly around our five chosen sites) and based on discussions with our local co-authors, taking into account their experience with heat (temperatures + humidity) and precipitation events. To further confirm our choice of November and August, we also performed an analysis of annual cycle of monthly historical temperatures from climate reanalysis, ERA5 [47], and precipitation rates from GPM [33] during PD (2008–2017) averaged over KSA and verified that November is the wettest month and July and August are the hottest months, while daytime relative humidity is slightly higher in August based on daytime AIRS [50] retrievals (not shown). AIRS is an infrared sounder aboard Aqua Satellite, and it provides data at 1° horizontal resolution. The monthly daytime relative humidity product from AIRS is available from NASA, and we used AIRS3STM v6 (https://disc.gsfc.nasa.gov/datasets/AIRS3STM_006/summary) [51]. Hence, while both are viable options, we chose to simulate August rather than July.

3. Results

3.1. Evaluation of the Downscaling Methodology

To evaluate our downscaling methodology, we focus on historical temperatures at 2 m and precipitation rates and compare our simulated climate fields from our WRF-ERA and WRF-PD simulations with the driving reanalysis product of WRF-ERA simulations and ERA5 for temperatures and with precipitation estimates from GPM and CRU for precipitation rates. WRF-ERA simulations show similar spatial structure and magnitude for mean temperatures at 2 m as ERA-Interim and ERA5 for both August and November (Figure 2). As expected, with the higher spatial resolution and shorter timesteps, effects of local spatial influences such as topography on temperatures are more pronounced in WRF-ERA compared to the driver reanalysis product. It is also evident that spatial distribution of temperatures in our WRF-ERA simulations shows closer resemblance to higher-resolution climate reanalysis ERA-5. Given the high spatial resolution (4 km) of the inner-most domain of the WRF-PD and WRF-ERA simulations, no gridded datasets at this granularity exist that can provide a commensurate landscape of the "observed" historical conditions; therefore, we cannot perform an unequivocal, quantitative assessment. However, the information provided by the more recent and high-resolution climate reanalysis product, ERA5, within our WRF model domain over the KSA region serves as a proxy for observed temperature variations. Hence, to further evaluate our downscaling setup, we calculated biases in temperatures between ERA5 and our downscaling simulations (WRF-PD and WRF-ERA) (Figure 3a–d). Statistically significant differences, tested using Student's *t*-test at 5% level, are indicated via stippling in Figure 3. While the spatial distribution of temperatures in both WRF-PD and WRF-ERA are simulated well compared to ERA5 for both months, there are statistically significant negative biases over the western side of KSA and positive biases over the eastern and northern parts of KSA in August. The cooler temperatures in WRF-ERA simulations along the Asir Mountains and the surrounding higher topography of the western part of KSA are clearly evident in August. Hence, these biases are likely due to the more detailed representation of the spatial features, and therefore, temperatures in WRF-ERA could indeed be an improvement over the ERA5 product. However, due to a lack of homogeneous, high-resolution gridded observational products in the region, we are unable to assess this further. In November, the negative biases are smaller in magnitude and extent along the western KSA in WRF-ERA simulations compared to August and even exhibit a narrow band of positive bias along the western coastline. Biases between WRF-ERA and ERA5 are more enhanced over the Empty Quarter in November. Furthermore, while the biases in WRF-ERA and WRF-PD simulations have similar signs and spatial structure over KSA, WRF-PD simulations have stronger positive biases compared to ERA5 in November. Nevertheless, both our CESM-driven WRF simulations (WRF-PD) and ERA-Interim-driven simulations (WRF-ERA) are able to capture the main features of the spatial distribution and magnitudes of mean historical temperatures at 2 m with stronger biases in November in WRF-PD.

As previously noted, August and November monthly precipitation rates from the WRF-ERA and WRF-PD simulations are assessed against interpolated measurements from CRU as well as GPM retrievals (Figure 4). Overall, the most significant spatial features of monthly precipitation rates over land in WRF-ERA and WRF-PD simulations are also seen in the CRU and GPM products (Figure 4). In particular, the precipitation maxima in November across central KSA, which extends coast-to-coast from the Red Sea to the Arabian Gulf, is prominent in both WRF simulations and GPM retrievals. In addition, the elevated precipitation rates in the southernmost regions of the AP are also clearly distinguishable in August. During both months, the enhanced precipitation rates as a result of the orographic effects of the Asir mountains are also prevalent. Furthermore, the persistent absence of precipitation or the lowest precipitation rates across the Empty Quarter (i.e., Rub' al Khali) are evident in both the WRF simulations and gridded observations/retrieval-based estimates. To further assess our downscaling, we calculated biases in daily precipitation rates between GPM and our downscaling simulations (WRF-PD and WRF-ERA) (Figure 3e–h). Both WRF-ERA and WRF-PD

yield statistically significantly enhanced precipitation rates over the Asir mountains in August, and this enhancement is more pronounced in the latter. WRF-PD is drier over the Empty Quarter in August. During the wet season, represented here as November, both WRF-ERA and WRF-PD produce similar positive biases with enhancements over higher topography along the western part of KSA. Quantitative differences in precipitation rates between our high-resolution WRF simulations (at 4 km) and observed/retrieved/reanalyzed products are expected due differences in horizontal resolution and uncertainties in observational products (see Section 2). Furthermore, the driver of our WRF-PD simulations is a CESM simulation that is not assimilated with observations after 1950, while the CESM fields that are input to our WRF simulations have been bias-corrected at NCAR [24,25]. As a result, some differences between WRF-PD and historical observational products are expected.

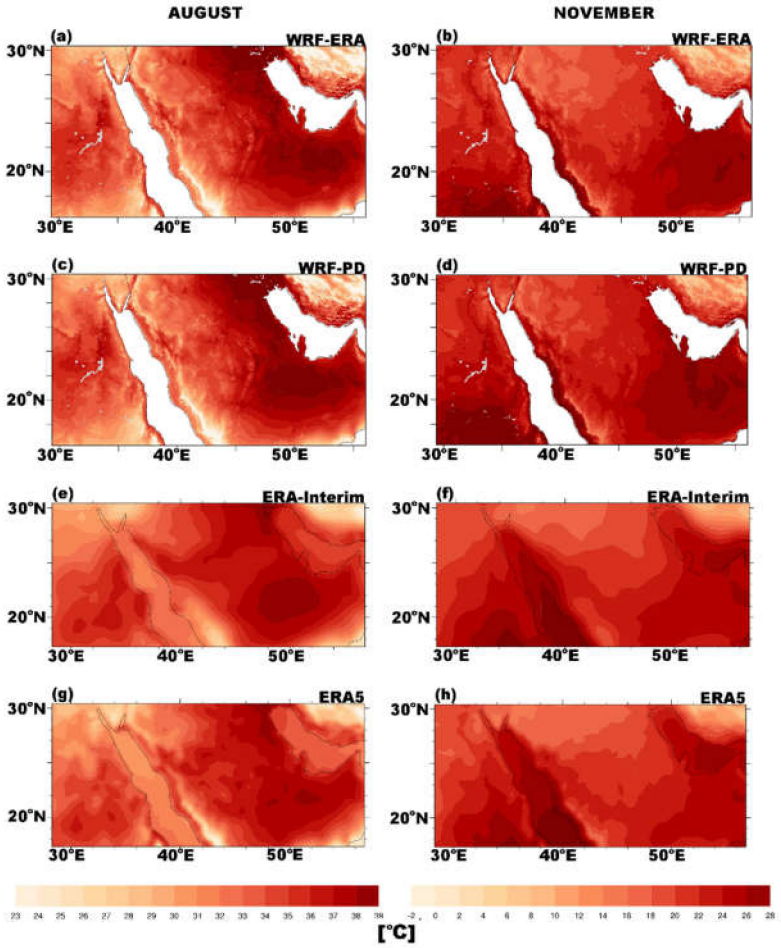

Figure 2. August (left) and November (right) daily mean temperatures at 2 m [°C] as simulated in WRF-ERA (**a**,**b**), WRF-PD (**c**,**d**) and from climate reanalysis ERA-Interim (**e**,**f**) and ERA5 (**g**,**h**).

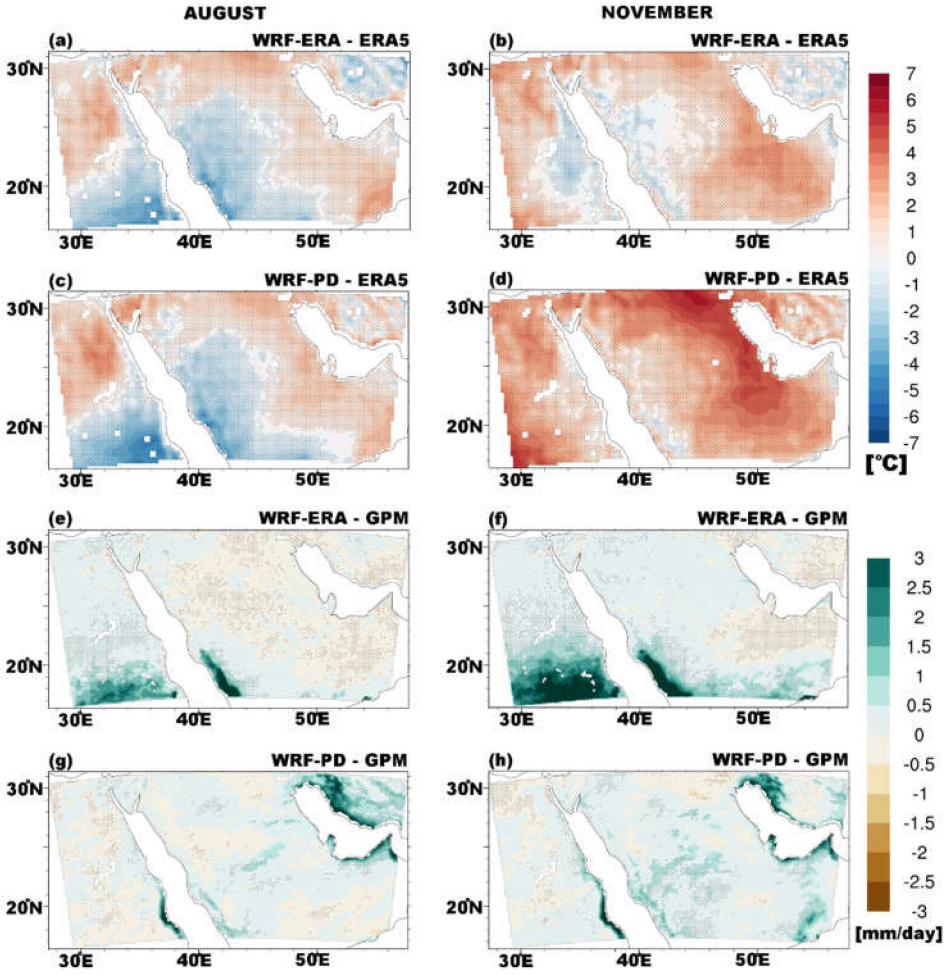

Figure 3. August (**left**) and November (**right**) biases in daily mean temperatures [°C] at 2 m between WRF-ERA and climate reanalysis ERA5 (**a**,**b**) and WRF-PD and ERA5 (**c**,**d**) and in precipitation rates [mm/day] between WRF-ERA and GPM (**e**,**f**) and WRF-PD and GPM (**g**,**h**). Statistically significant differences, tested using Student's *t*-test at 5% level, are indicated via stippling.

Due to the unique, sporadic nature of precipitation events in KSA, we also evaluated our model's ability to simulate day-to-day variability. In Figure 5, we compare day-to-day variations in precipitation rates at five local sites (see Section 2) averaged over 2008–2017 as simulated in WRF-PD and WRF-ERA with precipitation estimates from GPM. It is important to note that while our simulations are fed with climate reanalysis (ERA-Interim) or CESM at six-hourly intervals, our simulations have 15-day initialization time periods. Hence, due to the long nature of climate simulations and applied initialization time periods, we do not expect our downscaled fields to closely replicate historical day-to-day variations or an observed precipitation event to occur at the exact date in the simulations, but we do expect and intend to capture the sporadic nature of precipitation events and produce climatologically similar precipitation amounts within a given month/season. It is evident in Figure 5 that while for most sites our downscaling produces somewhat larger magnitudes of precipitation rates compared to GPM, our downscaling is able to capture the sporadic nature of precipitation and produce daily variability similar to that in GPM for both August and November.

All biases in the simulated historical climate variables, however small, should be taken into consideration when applying these projected changes of high-resolution climate fields in further applications (e.g., resilience and adaptation studies).

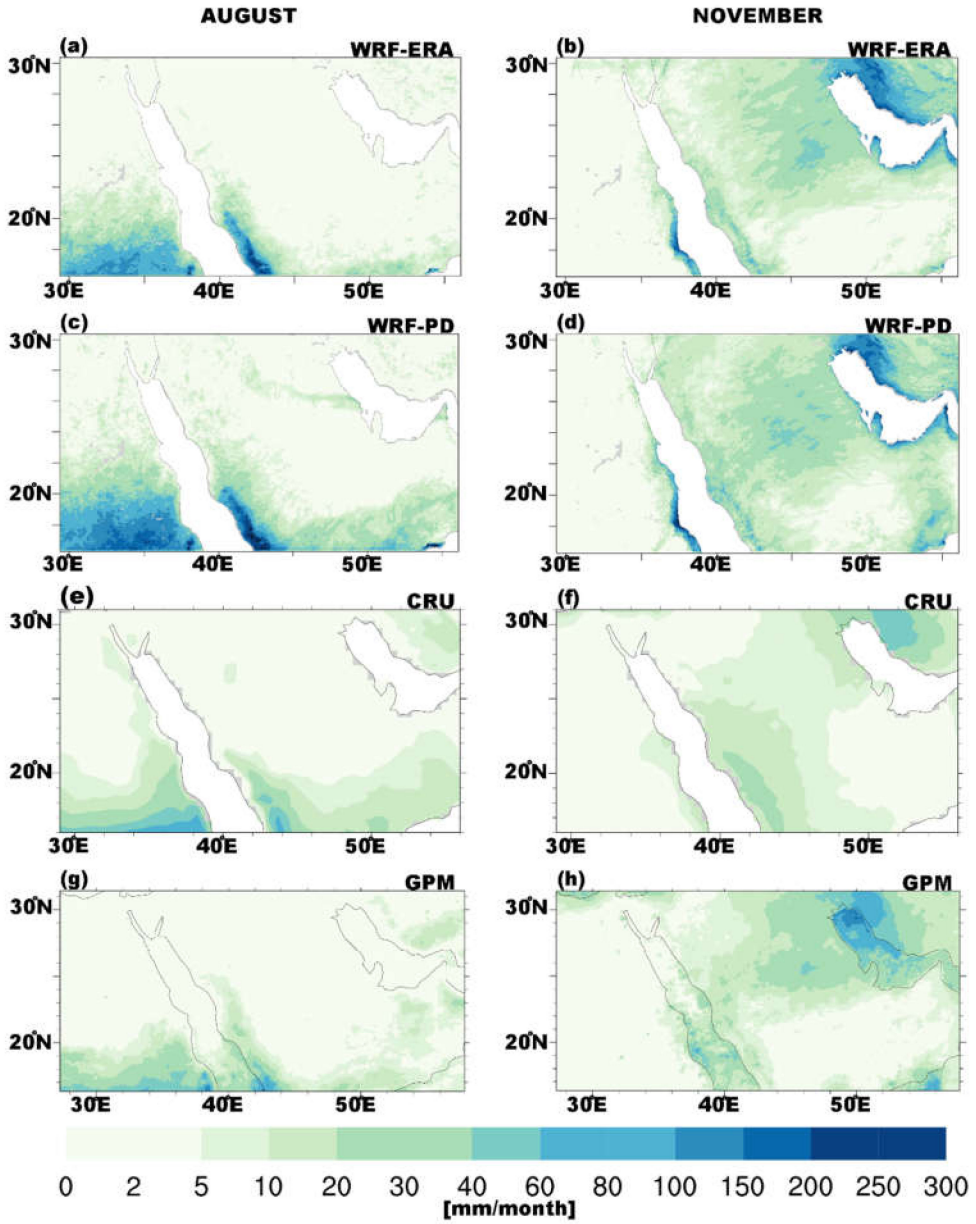

Figure 4. August (**left**) and November (**right**) monthly precipitation rates [mm/month] from WRF-ERA (**a**,**b**) and WRF-PD (**c**,**d**) simulations, CRU (**e**,**f**) and GPM (**g**,**h**).

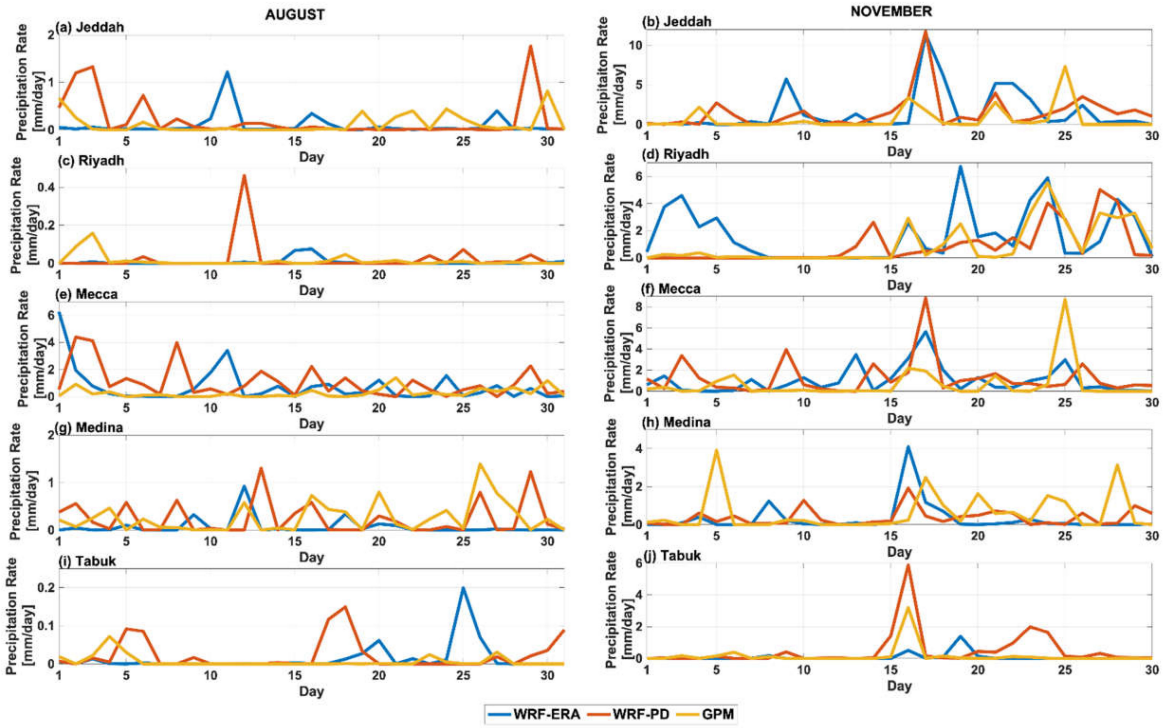

Figure 5. Day-to-day variation in precipitation rates (mm/day) in August (**left**) and November at five local sites, Jeddah (**a**,**b**), Riyadh (**c**,**d**), Makkah (**e**,**f**), Madinah (**g**,**h**), Tabuk (**i**,**j**), as simulated from WRF-ERA and WRF-PD and in retrievals from GPM averaged over 2008–2017.

3.2. Projected Future Changes

In this section, we present projected changes in the mean and extreme climate by mid-century focusing on 2-m temperatures and precipitation rates. Furthermore, we provide results from our local, city-level analysis of these changes.

3.2.1. Changes in the Mean Climate

We find that mean temperatures at 2 m increase in KSA by as much as 2 °C by mid-century in November and August compared to the historical time period (Figure 6a,b). Statistically significant differences in mean, maximum and minimum temperatures, tested using Student's *t*-test at 5% level, are indicated via stippling in Figure 6. Furthermore, we also find a marked skewness in the diurnal features of warming. The largest increases in daily maximum temperatures are seen across southwestern and central KSA in November (Figure 6d), while decreases in daily maximum temperatures are seen across the Asir mountains in August (Figure 6c). Conversely, August displays the largest increases in daily minimum temperatures, and these are seen across the northern and eastern regions of KSA. Unlike maximum temperatures, there are no decreases in minimum temperatures across KSA (Figure 6e,f).

Both precipitation rates and the number of rainy days increase in November across the northeastern regions of KSA by the middle of the 21st century (Figure 7b,d). Substantial decreases in November precipitation are seen across much of the southern portions of KSA, with significant decreases in the southwestern-most regions. Statistically significant differences, tested using Student's *t*-test at 5% level, are indicated via stippling in Figure 7. In contrast, there are strong increases in precipitation rates and the number of rainy days in August over the west coast of KSA (Figure 7a,c), and decreases across the northeast KSA and southeast AP.

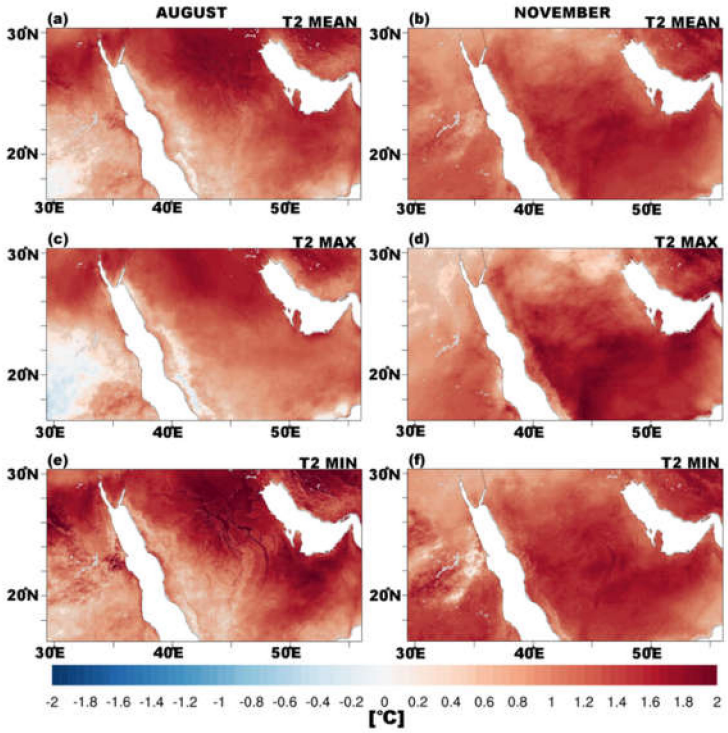

Figure 6. August (**left column**) and November (**right column**) changes in the mean (**a**,**b**), maximum (**c**,**d**) and minimum 2-m temperatures [°C] (**e**,**f**) between mid-century and present-day in high-resolution WRF simulations (WRF-MC–WRF-PD). Statistically significant differences, tested using Student's *t*-test at 5% level, are indicated via stippling.

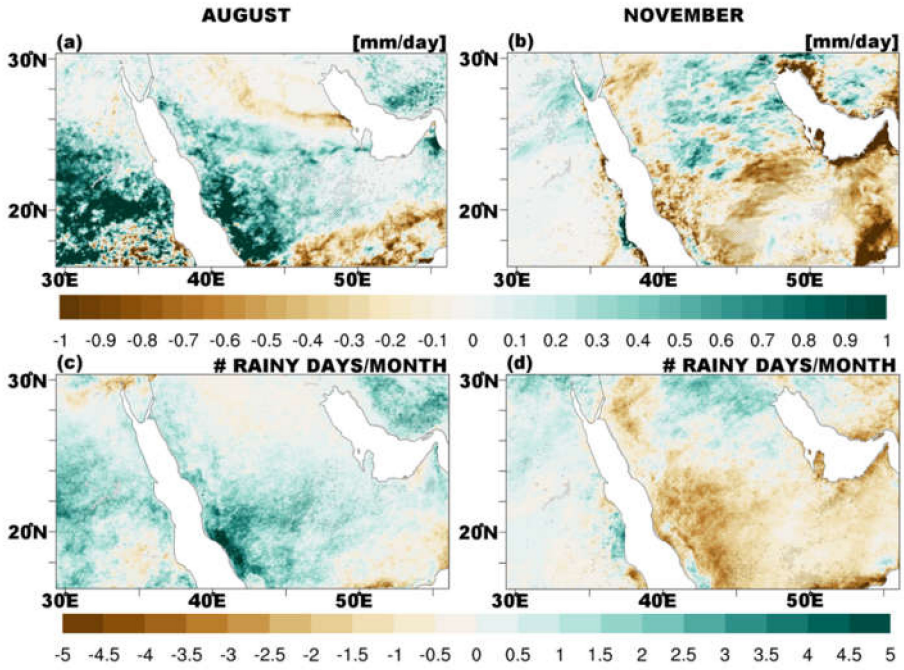

Figure 7. August (**left**) and November (**right**) changes in daily precipitation rates (**a**,**b**) and number of rainy days (**c**,**d**) between mid-century and present-day in high-resolution WRF simulations (WRF-MC–WRF-PD). Statistically significant differences, tested using Student's *t*-test at 5% level, are indicated via stippling.

3.2.2. Changes in the Extremes

Aside from the changes in mean fields, we also analyzed changes in the extreme temperatures and precipitation rates by the middle of the 21st century (Figure 8). We find that the 99th percentiles of 2-m daily maximum temperatures increase in November and August by as much as 3 °C by mid-century in our highest resolution domain (Figure 8a,b). In November, this increase is quite pronounced over the northern and northwestern parts of KSA, while in August, the increase in extreme temperatures is more uniform and slightly higher in the southern parts of KSA.

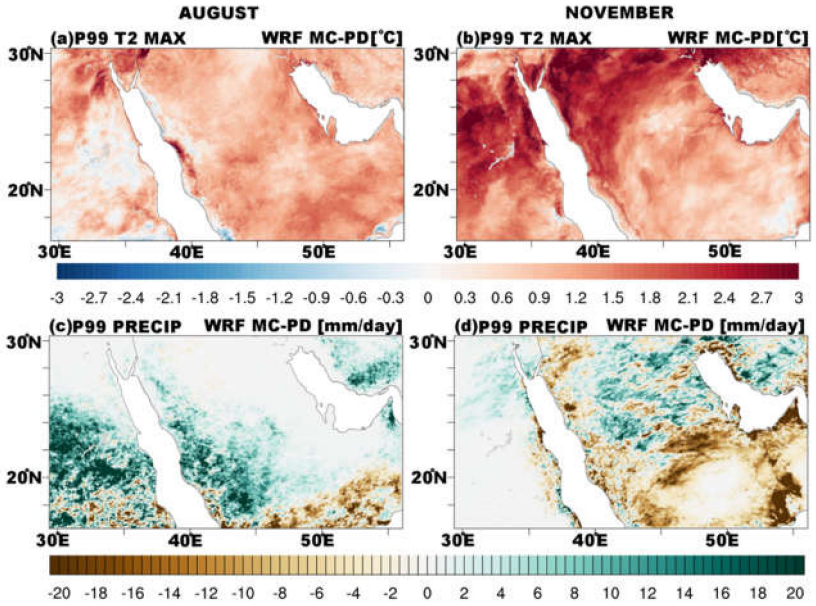

Figure 8. August (**left**) and November (**right**) changes in the 99th percentile (P99) of daily maximum temperatures [°C] (**a**,**b**) and precipitation rates [mm/day] (**c**,**d**) between mid-century and present-day in high-resolution WRF simulations (WRF-MC–WRF-PD).

For daily precipitation, we find that extreme rates increase over the western parts of KSA in August (Figure 8c), particularly along the coast of the Red Sea and surrounding the Asir Mountains, while a reduction is simulated over approximately the same area in November (Figure 8d). There is an increase in extreme precipitation rates by mid-century over some areas in the central and northeastern parts of KSA in November, while extreme precipitation rates over the same areas remain unchanged in August. Furthermore, across the northern flank of the Empty Quarter, there is a large region that experiences a reduction in extreme precipitation rates in November and along with the corresponding decreases in mean precipitation (Figure 7), this indicates a potential northward expansion of this extremely dry environment (toward Riyadh).

3.2.3. Projected Changes in Climate at Local, City Levels

To assess local, city-scale changes in climate, we focus on five strategic locations as described in Section 2. In Table 2 (3), we list daily means, 99th percentiles and number of days of exceedance of 99th percentile values (P99) for temperatures (accumulated precipitation rates) obtained in WRF-PD and WRF-MC simulations in November and August for the five cities. When analyzing local changes in these specific sites, we use mean values of the corresponding grid location as well as four grid points that surround it in the north–south and east–west directions.

Table 2. Daily means and 99th percentiles (p99) of 2-m temperatures (T2) from WRF-PD and WRF-MC, along with the number of days where daily temperatures exceed the 99th percentile of present-day (PD) value.

November	Daily Mean T2 (°C)		99th Percentile of T2 (°C)		# of Days Where T2 ≥ p99 of PD	
Local Site	**PD**	**MC**	**PD**	**MC**	**PD**	**MC**
Riyadh	23.6 ± 0.8	25.1 ± 1.3	29.3	30.1	0.3 ± 0.7	1.2 ± 1.6
Jeddah	29.1 ± 0.3	30.3 ± 0.4	31.8	33	0.3 ± 0.5	2.6 ± 1.6
Makkah	27.4 ± 0.6	28.6 ± 0.6	30.5	32.5	0.3 ± 0.5	3.6 ± 2.1
Madinah	24.5 ± 0.6	25.8 ± 1	28.4	30.9	0.3 ± 0.8	3.9 ± 2.4
Tabuk	20 ± 0.9	21.3 ± 0.6	25.7	28.7	0.3 ± 0.5	2.5 ± 2.3
August	**Daily Mean T2 (°C)**		**99th Percentile of T2 (°C)**		**# of Days Where T2 ≥ p99 of PD**	
Local Site	**PD**	**MC**	**PD**	**MC**	**PD**	**MC**
Riyadh	37.4 ± 0.5	38.7 ± 0.6	40.4	41.3	0.3 ± 0.5	4.4 ± 2.9
Jeddah	32.8 ± 0.4	33.6 ± 0.3	34.7	35.7	0.3 ± 0.5	3 ± 2.3
Makkah	32 ± 1.0	32.6 ± 0.7	35.8	37	0.3 ± 0.3	1.8 ± 1.7
Madinah	34.6 ± 0.8	35.2 ± 0.5	39.5	39.7	0.3 ± 0.7	0.4 ± 0.6
Tabuk	32.8 ± 0.8	34.1 ± 0.6	37.7	38.9	0.3 ± 0.5	1.9 ± 1.4

Both mean and extreme temperatures at 2 m increase for all sites in August and November by as much as 1.5 °C (Table 2). The change in mean 2-m temperatures by mid-century nearly doubles in November compared to the change in August (except for the case of Riyadh, where change remains high and the same). The change in extreme temperatures at 2 m reaches as much as 3 °C in November in Tabuk and is generally less pronounced in August compared to November. The number of days where temperatures are greater than or equal to the 99th percentile of its present-day value (PD) increases substantially for all locations and by more than 10-fold its PD value for some locations (except for a modest increase in Madinah in August). Overall, we find that temperature extremes become more intense and more frequent for all locations.

Changes in mean precipitation rates by mid-century are more subtle while confidence intervals are larger when compared to changes in temperatures as expected in an arid climate (Table 3). Larger confidence intervals are partially due to the limited number of years simulated. By mid-century, precipitation rates increase for all locations in August. Precipitation rates decrease in November for Jeddah, Makkah and Tabuk. Makkah and Tabuk experience less intense and less frequent extremes in November by mid-century. The intensity and frequency of precipitation extremes increase for all sites in August, and changes are more pronounced compared to November.

August is one of the months where prolonged heat extremes are observed (e.g., [1]). Hence, under a warmer climate, continuing daily work/life activities while preserving health and well-being of residents and visitors could be challenging in the region. To understand how heat extremes will affect daily activities, health and well-being of the residents by mid-century, we calculated heat index following U.S. National Weather Service (NWS) [52–54]. Heat index represents combined influences of temperature and humidity under calm winds in shade and is a measure of apparent ("feels-like") temperature (e.g., [53]). The inclusion of humidity and human physiological factors in the heat index calculation makes it a more relevant measure of human discomfort than the effects of temperatures alone (e.g., [52]).

We present August maximum Heat Index (AHI) values averaged over mid-century (MC) and present-day (PD) time periods in Table 4. AHI is greater than 41 °C (105 °F) for all sites (except for Tabuk), which indicates that in the present-day climate, heatstroke and heat exhaustion are "likely" (when HI ≥ 41 °C). We find that heat index increases for all sites by mid-century by 2 to 3 °C in August. Despite this increase, AHI stays below the dangerously high levels (≥54 °C or 130 °F) at mid-century for all locations except for Jeddah, where it is found that these dangerous health conditions may occur on average at least a day every August as opposed to one day every ten years in the present climate.

Table 3. Daily accumulated precipitation rates and 99th percentiles (p99) of precipitation rates from WRF-PD and WRF-MC, along with the number of days where daily precipitation rates exceed the 99th percentile of present-day (PD) value.

November	Daily Precipitation Rate [mm/day]		99th Percentile of Daily Precipitation [mm/day]		# of Days Where Precipitation Rate ≥ p99 of PD	
Local Site	**PD**	**MC**	**PD**	**MC**	**PD**	**MC**
Riyadh	0.9 ± 0.8	1.1 ± 1.2	20.1	29.6	0.3 ± 0.3	0.6 ± 0.7
Jeddah	1.5 ± 1.2	0.9 ± 1.0	24.6	25.4	0.3 ± 0.4	0.3 ± 0.5
Makkah	1.2 ± 0.7	1.0 ± 0.5	22.9	14.5	0.3 ± 0.3	0 ± 0
Madinah	0.4 ± 0.2	0.5 ± 0.4	8.9	12.4	0.3 ± 0.5	0.5 ± 0.7
Tabuk	0.5 ± 0.5	0.2 ± 0.3	16.2	6.2	0.3 ± 0.3	0.1 ± 0.2
August	**Daily Precipitation Rate [mm/day]**		**99th Percentile of Daily Precipitation [mm/day]**		**# of Days Where Precipitation Rates ≥ p99 of PD**	
Local Site	**PD**	**MC**	**PD**	**MC**	**PD**	**MC**
Riyadh	0.02 ± 0.03	0.3 ± 0.4	0.42	8.72	0.3 ± 0.5	1 ± 1.1
Jeddah	0.2 ± 0.3	0.8 ± 0.6	9.1	21.1	0.3 ± 0.7	1 ± 0.7
Makkah	1.0 ± 1.4	1.8 ± 0.9	22.32	33.35	0.3 ± 0.5	0.8 ± 0.6
Madinah	0.2 ± 0.3	0.6 ± 0.4	6.9	13.7	0.3 ± 0.5	1.1 ± 0.5
Tabuk	0.02 ± 0.03	0.1 ± 0.1	0.9	4.64	0.3 ± 0.5	0.6 ± 0.6

Table 4. Daily maximum heat index for August from WRF-PD and WRF-MC, along with the number of days where daily maximum heat index exceeds 54 °C.

August	Mean of Daily Maximum August NWSHeat Index (AHI) [°C]		Frequency of Days Daily Max AHI > 54 °C	
Local Site	**PD**	**MC**	**PD**	**MC**
Riyadh	43.5 ± 0.8	45.6 ± 0.8	0	0
Jeddah	46.6 ± 1.1	44.1 ± 1.1	0.1 ± 0.2	1.5 ± 1.9
Makkah	42 ± 1.2	44.3 ± 0.7	0	0
Madinah	42.4 ± 1.2	44 ± 0.8	0	0
Tabuk	38.9 ± 1.2	40.6 ± 1	0	0

4. Discussion and Conclusions

Higher-resolution convection-permitting modeling and climate projections like the ones we present in this paper, while quite informative, come at great computational expense and are currently beyond reach for the majority of research institutions across the world. Hence, we were only able to simulate selected decadal periods and downscale projections from only one ESM under a single scenario. Nevertheless, they provide a higher-resolution glimpse into the potential changes in climate that might occur in the region and help regional decision-makers, engineers and urban designers in local adaptation efforts.

Our results reveal that our downscaling setup is able to capture the spatial structure of historical temperatures and precipitation rates. The biases with respect to gridded observations-based products we find between our downscaled products and ERA5 for the historical time period (2008–2017) in August are similar to the biases obtained in the downscaling simulations of Syed et al. 2019 [9] for the dry season for CORDEX MENA and CORDEX SA simulations (between 1975 and 2005). However, it is difficult to make a direct comparison with our results due to the differences in the horizontal resolution (i.e., 4 km in ours vs. 50 km in theirs) and model setup of WRF simulations, lengths of historical time periods and months studied (i.e., one month in our simulations vs. dry season (May–October) in their study) and blends of observational products used in the two studies. Furthermore, their downscaling is from ERA40, which is the predecessor of the driving field (ERA-Interim) of our WRF-ERA simulations.

Our results reveal significant differences in the mean and extreme temperatures and precipitation rates by mid-century in KSA between dry-hot August and wet November months. We studied changes across the peninsula and around five sites of local significance across the Kingdom. We find increasing

temperatures by mid-century across KSA and the AP as well as for all five local sites in both August and November. Downscaling three ESMs using a regional climate model, Almazroui et al. (2019) [6] found 0.6 °C per decade change in Makkah, 0.57 °C per decade change in Madinah and 0.7 °C per decade change in Riyadh when comparing their mid-century simulations (2021–2050) to their historical simulations (1961–2000) [6]. Here, we find 1.3, 1.2 and 1.5 °C per decade change in temperatures (Table 2) in our mid-century simulations (2041–2050) compared to our simulations for the historical period (2008–2017) for Madinah, Makkah and Riyadh, respectively. However, these results are not comparable due to the different definitions of mid-century and historical time periods. They also used a coarser, 50 km, horizontal resolution regional climate modeling approach, which differed from ours, and they used a different regional climate model and downscaled different ESMs [6].

While mean precipitation rates increase along the western coastal region of KSA in August, the same region experiences reduction in precipitation rates in November. Furthermore, mean precipitation rates increase in August by mid-century for all five sites, while some sites experience reduction in precipitation rates by mid-century in November. Additionally, we find a strong consistency in the patterns of change in mean precipitation rates and the number of rainy days, which indicates that mean changes are more strongly influenced by the occurrence (and absence) of precipitation on any given day as opposed to changes in the intensity of precipitation events. The increases we find in the projected precipitation rates along the coastal western AP are consistent with the observed historical trends in precipitation rates between 1978 and 2009 in Almazroui et al. (2012) [3].

In addition to increasing mean precipitation rates, we also find increasing extreme precipitation rates in August by mid-century along the coast of Red Sea as well as increased frequency of extreme precipitation events at all five local sites. Conversely, the northern flank of the Empty Quarter experiences a noticeable reduction in extreme and mean precipitation rates during November (typically the wettest part of the year), which would support a potential northward expansion (toward the higher-populated areas near Riyadh) of this extremely dry environment. However, in the context of a proactive adaptation strategy at scale (i.e., commensurate to the transport of desalinized water across KSA), the increases in mid-century August precipitation rates along the western mountainous coast of the AP indicate that water could be harvested, used to recharge local aquifers and transported from this region to areas of KSA that will likely require increased supply to meet increased water demands across the domestic, agricultural and industrial sectors. Our high-resolution climate simulations are able to more explicitly resolve the impacts of the Asir Mountains to increase precipitation, hence, our results signify that water harvesting from this locality should be considered as a viable consideration of adapting to water scarcity under climate change to increase the habitability, livability and economic resiliency of the region.

Health, quality of life and continuation of daily activities and businesses are also of concern under a warmer world in a region that already is classified as a desert climate. We found that the August maximum heat index is already high in the region, and prolonged exposure to heat is likely to cause heatstroke. While heat index is found to increase by mid-century in our simulations, it does not reach levels where heatstroke is imminent, except for Jeddah. Here, we find increasing frequency of occurrence of dangerous heat index conditions in our simulations, suggesting that changes and improvements to local design of houses and workplaces will be necessary to protect human health and increase local habitability and resilience.

We hope the results of our study will inspire researchers to continue working on the simulations to extend the simulation period and include more climate scenarios as well as more ESMs for downscaling. These extensions would provide a more comprehensive picture of potential changes in the mean and extreme climate in the region, hence enable more complete insights on improving local and regional resilience under climate change and changing extremes.

Author Contributions: Conceptualization, methodology, funding acquisition, data curation, computational setup, computational experiments, investigation, formal analysis, visualization and writing, M.K.; conceptualization,

funding acquisition and writing—reviewing and editing, C.A.S. and A.A.; data curation, I.A., T.A. and W.A.; funding acquisition, K.S. All authors have read and agreed to the published version of the manuscript.

Funding: Funding for this project was provided through the Center for Complex Engineering Systems (CCES) at the King Abdulaziz City for Science and Technology (KACST) and the Massachusetts Institute of Technology (MIT).

Acknowledgments: We acknowledge the computational support Greg Shomo and Jeffrey R. Scott provided to our project on MIT's Svante High Performance Computing System. M. Komurcu would like to acknowledge treasured discussions on remapping of high-resolution climate fields with Matthew Huber of Purdue University and Ufuk Utku Turuncuoglu of NCAR. Authors would like to acknowledge the three anonymous reviewers whose comments greatly improved this study.

Conflicts of Interest: The authors declare no conflicts of interest.

References

1. Alsarhan, A.; Zatari, T.; Al-Asaly, M.; Mirza, K.; Harthi, A.; Othman, M.; Babiker, M.; Khan, A.; Aljabr, A.; Albuqami, F.; et al. Third National Communication of the Kingdom of Saudi Arabia. 2016. Available online: https://unfccc.int/files/national_reports/non-annex_i_natcom/application/pdf/saudi_arabia_nc3_22_dec_2016.pdf (accessed on 19 September 2020).
2. Rehman, S.; Al-Hadhrami, L. Extreme Temperature Trends on the West Coast of Saudi Arabia. *Atmos. Clim. Sci.* **2012**, *2 No. 3*, 351–361. [CrossRef]
3. Almazroui, M.; Nazrul Islam, M.; Athar, H.; Jones, P.D.; Rahman, M.A. Recent climate change in the Arabian Peninsula: Annual rainfall and temperature analysis of Saudi Arabia for 1978–2009. *Int. J. Clim.* **2012**, *32*, 953–966. [CrossRef]
4. Almazroui, M.; Islam, M.N.; Dambul, R.; Jones, P.D. Trends of temperature extremes in Saudi Arabia. *Int. J. Clim.* **2014**, *34*, 808–826. [CrossRef]
5. Donat, M.G.; Peterson, T.C.; Brunet, M.; King, A.D.; Almazroui, M.; Kolli, R.K.; Boucherf, D.; Al-Mulla, A.Y.; Nour, A.Y.; Aly, A.A.; et al. Changes in extreme temperature and precipitation in the Arab region: Long-term trends and variability related to ENSO and NAO. *Int. J. Clim.* **2014**, *34*, 581–592. [CrossRef]
6. Almazroui, M. Temperature Changes over the CORDEX-MENA Domain in the 21st Century Using CMIP5 Data Downscaled with RegCM4: A Focus on the Arabian Peninsula. *Adv. Meteor.* **2019**, *2019*, 1–18. [CrossRef]
7. Tarawneh, Q.Y.; Chowdhury, S. Trends of Climate Change in Saudi Arabia: Implications on Water Resources. *Climate* **2018**, *6*, 8. [CrossRef]
8. Bucchignani, E.; Mercogliano, P.; Panitz, H.-J.; Montesarchio, M. Climate change projections for the Middle East–North Africa domain with COSMO-CLM at different spatial resolutions. *Adv. Clim. Change. Res.* **2018**, *9*, 66–80. [CrossRef]
9. Syed, F.S.; Latif, M.; Al-Maashi, A.; Gluham, A. Regional climate model RCA4 simulations of temperature and precipitation over the Arabian Peninsula: Sensitivity to CORDEX domain and lateral boundary conditions. *Clim. Dyn.* **2019**, *53*, 7045–7064. [CrossRef]
10. Buzan, J.R.; Huber, M. Moist Heat Stress on a Hotter Earth. *Annu. Rev. Earth Planet. Sci.* **2020**, *48*, 623–655. [CrossRef]
11. Pal, J.; Eltahir, E. Future temperature in southwest Asia projected to exceed a threshold for human adaptability. *Nat. Clim. Chang.* **2011**, *6*, 197–200. [CrossRef]
12. Mashat, A.; Basset, H.A. Analysis of Rainfall over Saudi Arabia, JKAU: Met. *Env. Arid. Land. Agric. Sci.* **2011**, *22*, 59–78. [CrossRef]
13. Yesubabu, V.; Srinivas, C.V.; Langodan, S.; Hoteit, I. Predicting extreme rainfall events over Jeddah, Saudi Arabia: Impact of data assimilation with conventional and satellite observations. *Q.J.R. Meteorol. Soc.* **2016**, *142*, 327–348. [CrossRef]
14. De Vries, A.J.; Feldstein, S.B.; Riemer, M.; Tyrlis, E.; Sprenger, M.; Baumgart, M.; Fnais, M.; Lelieveld, J. Dynamics of tropical–extratropical interactions and extreme precipitation events in Saudi Arabia in autumn, winter and spring. *Q. J. R. Meteorol. Soc.* **2016**, *142*, 1862–1880. [CrossRef]
15. Momani, N.M.; Fadil, A.S. Changing public policy due to Saudi city of Jeddah flood disaster. *J. Soci. Sci.* **2010**, *6*, 424–428. [CrossRef]
16. Daoudi, M.; Niang, A.J. *Flood Risk and Vulnerability of Jeddah City, Saudi Arabia, Recent Advances in Flood Risk Management*; Intech Open: London, UK, 2018; pp. 634–654.

17. Şen, Z.; Al Alsheikh, A.; Al-Turbak, A.S.A.M.; Al-Bassam, A.M.; Al-Dakheel, L. Climate change impact and runoff harvesting in arid regions. *Arab. J. Geosci.* **2013**, *6*, 287–295. [CrossRef]
18. Sebai, Z.A. Malaria in Saudi Arabia. *Trop. Doc.* **1998**, *18*, 183–188. [CrossRef] [PubMed]
19. Almazroui, M. Simulation of present and future climate of Saudi Arabia using a regional climate model (PRECIS). *Int. J. Clim.* **2013**, *33*, 2247–2259. [CrossRef]
20. Deng, L.; McCabe, M.F.; Stenchikov, G.; Evans, J.P.; Kucera, P.A. Simulation of Flash-Flood-Producing Storm Events in Saudi Arabia Using the Weather Research and Forecasting Model. *J. Hydrometeor.* **2015**, *16*, 615–630. [CrossRef]
21. Alsarraf, H.; Broeke, M.V.D. Using the WRF Regional Climate Model to Simulate Future Summertime Wind Speed Changes over the Arabian Peninsula. *J. Clim. Weather Forecast.* **2015**, *3*, 144. [CrossRef]
22. Komurcu, M.; Emanuel, K.A.; Huber, M.; Acosta, R.P. High-resolution climate projections for the northeastern United States using dynamical downscaling at convection-permitting scales. *Earth Space Sci.* **2018**, *5*, 801–826. [CrossRef]
23. Almazroui, M. Calibration of TRMM rainfall climatology over Saudi Arabia during 1998–2009. *Atmos Res.* **2011**, *99*, 400–414. [CrossRef]
24. Bruyère, C.L.; Done, J.M.; Holland, G.J.; Fredrick, S. Bias corrections of global models for regional climate simulations of high-impact weather. *Clim. Dynam.* **2014**, *43*, 1847–1856. [CrossRef]
25. Bruyère, C.L.; Monaghan, A.J.; Steinhoff, D.F.; Yates, D. *Bias-Corrected CMIP5 CESM Data in WRF/MPAS Intermediate File Format*; (Technical Report TN-515+STR, 27); National Center for Atmospheric Research: Boulder, CO, USA, 2015.
26. Skamarock, W.C.; Klemp, J.B.; Dudhia, J.; Gill, D.O.; Barker, D.M.; Duda, M.; Huang, X.-Y.; Wang, W. *A Description of the Advanced Research WRF Version 3*; (Technical Note NCAR/TN-475+STR); National Center for Atmospheric Research: Boulder, CO, USA, 2008.
27. Dezfuli, A.K.; Zaitchik, B.F.; Badr, H.S.; Evans, J.; Peters-Lidard, C.D. The Role of Low-Level, Terrain-Induced Jets in Rainfall Variability in Tigris–Euphrates Headwaters. *J. Hydrometeor.* **2017**, *18*, 819–835. [CrossRef] [PubMed]
28. Prein, A.; Rasmussen, R.M.; Ikeda, K.; Liu, C.; Klark, M.P.; Holland, G.J. The future intensification of hourly extremes. *Nat. Clim. Change* **2017**, *7*, 48–52. [CrossRef]
29. Attada, R.; Dasari, H.P.; Kunchala, R.K.; Langodan, S.; Niranjan Kumar, K.; Knio, O.; Hoteit, I. Evaluating Cumulus Parameterization Schemes for the Simulation of Arabian Peninsula Winter Rainfall. *J. Hydrometeor.* **2012**, *21*, 1089–1114. [CrossRef]
30. Kain, J.S. The Kain–Fritsch convective parameterization: An update. *J. Appl. Meteorol. Climatol.* **2004**, *43*, 170–181. [CrossRef]
31. Hong, S.; Lim, J. The WRF Single-Moment 6-Class Microphysics Scheme (WSM6). *J. Korean Meteorol. Soci.* **2006**, *42*, 129–151.
32. Oleson, K.W.; Lawrence, D.M.; Bonan, G.B.; Flanner, M.G.; Kluzek, E.; Lawrence, P.J.; Levis, S.; Swenson, S.C.; Thornton, P.J.; Dai, A.; et al. *Technical Description of Version 4 of the Community Land Model (CLM)*; (Technical Note NCAR/TN–478+STR); National Center for Atmospheric Research: Boulder, CO, USA, 2010.
33. Hong, S.Y.; Noh, Y.; Dudhia, J. A new vertical diffusion package with an explicit treatment of entrainment processes. *Mon. Weather Rev.* **2006**, *134*, 2318–2341. [CrossRef]
34. Iacono, M.J.; Delamere, J.S.; Mlawer, E.J.; Shephard, M.W.; Clough, S.A.; Collins, W.D. Radiative forcing by long-lived greenhouse gases: Calculations with the AER radiative transfer models. *J. Geophy. Res.* **2008**, *113*, D13103. [CrossRef]
35. Monaghan, A.J.; Steinhoff, D.F.; Bruyere, C.L.; Yates, D. NCAR CESM Global Bias-Corrected CMIP5 Output to Support WRF/MPAS Research. Research Data Archive at the National Center for Atmospheric Research. Computational and Information Systems Laboratory. 2014. Available online: https://doi.org/10.5065/D6DJ5CN4 (accessed on 19 September 2020).
36. Dee, D.P.; Uppala, S.M.; Simmons, A.J.; Berrisford, P.; Poli, P.; Kobayashi, S.; Andrae, U.; Balmasedo, M.A.; Balsamo, G.; Bauer, P.; et al. The ERA-Interim reanalysis: Configuration and performance of the data assimilation system. *Quart. J. Royal. Meteorol. Soc.* **2011**, *137*, 553–597. [CrossRef]

37. European Centre for Medium-Range Weather Forecasts. ERA-Interim Project, Single Parameter 6-Hourly Surface Analysis and Surface Forecast Time Series. Research Data Archive at the National Center for Atmospheric Research, Computational and Information Systems Laboratory. 2012. Available online: https://doi.org/10.5065/D64747WN (accessed on 7 January 2020).
38. Lorenz, C.; Kunstmann, H. The hydrological cycle in three state-of-the-art reanalyses: Intercomparison and performance analysis. *J. Hydrometeor.* **2012**, *13*, 1397–1420. [CrossRef]
39. Soares, P.M.M.; Cardoso, R.M.; Miranda, P.M.A.; de Medeiros, J.; Belo-Pereira, M.; Espirito-Santo, F. WRF high resolution dynamical downscaling of ERA-Interim for Portugal. *Clim. Dynam.* **2012**, *39*, 2497–2522. [CrossRef]
40. Bieniek, P.A.; Bhatt, U.S.; Walsh, J.E.; Rupp, T.S.; Zhang, J.; Krieger, J.R.; Lader, R. Dynamical downscaling of ERA-Interim temperature and precipitation for Alaska. *J. Appl. Meteorol. Clim.* **2015**, *55*, 635–654. [CrossRef]
41. Almazroui, M. RegCM4 in climate simulation over CORDEX-MENA/Arab domain: Selection of suitable domain, convection and land-surface schemes. *Int. J. Clim.* **2016**, *36*, 236–251. [CrossRef]
42. Sun, Q.; Miao, C.; Duan, Q.; Ashouri, H.; Sorooshian, S.; Hsu, K.-L. A review of global precipitation data sets: Data sources, estimation, and intercomparisons. *Rev. Geophy.* **2018**, *56*, 79–107. [CrossRef]
43. Flato, G.; Marotzke, J.; Abiodun, B.; Braconnot, P.; Chou, S.C.; Collins, W.; Cox, P.; Driouech, F.; Emori, S.; Eyring, V.; et al. *Climate Change 2013: The Physical Science Basis. Contribution of Working Group I to the Fifth Assessment Report of the Intergovernmental Panel on Climate Change (9)*; Cambridge University Press: Cambridge, UK, 2013; pp. 741–866.
44. Hartmann, D.L.; Klein Tank, A.M.G.; Rusticucci, M.; Alexander, L.V.; Broönnimann, S.; Charabi, Y.; Dentener, F.J.; Dlugokencky, E.J.; Easterling, D.R.; Kaplan, A.; et al. Observations: Atmosphere and Surface. In *Climate Change 2013: The Physical Science Basis. Contribution of Working Group I to the Fifth Assessment Report of the Intergovernmental Panel on Climate Change*; Cambridge University Press: Cambridge, UK, 2013; Volume 96, pp. 159–254.
45. Hou, A.Y.; Kakar, R.K.; Neeck, S.; Azarbarzin, A.A.; Kummerow, C.D.; Kojima, M.; Iguchi, T. The global precipitation measurement mission. *Bull. Amer. Meteorol. Soci.* **2014**, *95*, 701–722. [CrossRef]
46. Harris, I.; Osborn, T.J.; Jones, P.; Lister, D. Version 4 of the CRU TS monthly high-resolution gridded multivariate climate dataset. *Sci. Data* **2020**, *7*, 109. [CrossRef]
47. Hersbach, H.; Bell, B.; Berrisford, P.; Hirahara, S.; Horanyi, A.; Munoz-Sabater, J.; Nicolas, J.; Peubey, C.; Radu, R.; Schepers, D.; et al. The ERA5 global reanalysis. *Q. J. R. Meteorol. Soci.* **2020**, *146*, 1999–2049. [CrossRef]
48. Huffman, G.J.; Stocker, E.F.; Bolvin, D.T.; Nelkin, E.J.; Jackson, T. *GPM IMERG Final Precipitation L3 1 day 0.1 degree × 0.1 degree V06*; Savtchenko, A., Ed.; Goddard Earth Sciences Data and Information Services Center (GES DISC): Greenbelt, MD, USA, 2019. Available online: https://doi.org/10.5067/gpm/imergdf/day/06 (accessed on 19 September 2020).
49. European Centre for Medium-Range Weather Forecasts. Updated Monthly. ERA5 Reanalysis (0.25 Degree Latitude-Longitude Grid). Research Data Archive at the National Center for Atmospheric Research. Computational and Information Systems Laboratory. 2019. Available online: https://doi.org/10.5065/BH6N-5N20 (accessed on 19 September 2020).
50. Kahn, B.H.; Irion, F.W.; Dang, V.T.; Manning, E.M.; Nasiri, S.L.; Naud, C.M.; Blaisdel, J.M.; Schreier, M.M.; Yue, Q.; Bowman, K.W.; et al. The Atmospheric Infrared Sounder Version 6 Cloud Products. *Atoms. Chem. Phys.* **2014**, *1*. [CrossRef]
51. AIRS Science Team/Joao Teixeira. *AIRS/Aqua L3 Monthly Standard Physical Retrieval (AIRS-only) 1 degree × 1 degree V006*; Goddard Earth Sciences Data and Information Services Center (GES DISC): Greenbelt, MD, USA, 2013. Available online: https://disc.gsfc.nasa.gov/datasets/AIRS3STD_006/summary (accessed on 19 September 2020).
52. Buzan, J.R.; Oleson, K.; Huber, M. Implementation of a suite of heat stress metrics within the Community Land Model version 4.5. *Geosi. Model Dev.* **2015**, *8*, 151–170. [CrossRef]

53. Steadman, T.G. The assessment of sultriness, Part I: A temperature-humidity index based on human physiology and clothing science. *J. Appl. Meteorol.* **1979**, 18. [CrossRef]
54. Rothfusz, L.P. National Weather Service Technical Attachment (SR 90-24). 1990. Available online: https://www.weather.gov/media/wrh/online_publications/TAs/ta9024.pdf (accessed on 19 September 2020).